Electronic structure and magnetic properties of hole-carrier-doped La_2MnNiO_6:$La_{2-x}Sr_xMnNiO_6$

Bongjae Kim, Hong Chul Choi, Beom Hyun Kim, and B. I. Min
PCTP, Department of Physics, Pohang University of Science and Technology, Pohang 790-784, Korea
(Received 27 November 2009; revised manuscript received 30 March 2010; published 1 June 2010)

We have investigated hole-carrier-doping effects in a ferromagnetic insulator La_2MnNiO_6. Employing the *ab initio* band-structure method, we have examined the changes in the electronic structures and the valence states of Sr-doped $La_{2-x}Sr_xMnNiO_6$ with varying Sr doping ratio. On Sr doping, we have found a transition from a ferromagnetic insulating phase to a half-metallic phase. The half-metallic nature in $La_{2-x}Sr_xMnNiO_6$ is found to be robust with respect to the on-site Coulomb correlation of transition metal 3*d* electrons and the antisite disorder at *B* sites. We have corroborated that the substantially weak x-ray magnetic circular dichroism signal observed for $La_{2-x}Sr_xMnNiO_6$, as compared to the undoped system, is caused by antisite disorder at *B* sites in a Sr-doped system.

DOI: 10.1103/PhysRevB.81.224402 PACS number(s): 71.20.Eh, 75.50.−y

I. INTRODUCTION

Double perovskite La_2MnNiO_6 is known to be a ferromagnetic (FM) insulator having the highest Curie temperature $T_C \sim 280$ K among FM insulators.[1,2] The FM ordering of Ni and Mn spins in this material is considered to be a typical example of the Goodenough-Kanamori-Anderson (GKA) rules for the superexchange interaction.[3,4] Recent theoretical and experimental attraction has been drawn to this material both in bulk and film form because of being a possible candidate of spintronic materials.[5–25] In double perovskite $A_2B'B''O_6$, *B*-site transition metal (TM) elements (Mn and Ni for La_2MnNiO_6) are influenced by the octahedral crystal field from neighboring oxygen ions. After long controversy,[1,26–31] the valence states of Mn and Ni have been found to be tetravalent (Mn^{4+}) and divalent (Ni^{2+}) with orbital occupation of t_{2g}^3 and $t_{2g}^6e_g^2$, respectively.[6,7,16,17,24]

There have been many investigations on effects of *A*-site doping in double perovskite $A_2B'B''O_6$. For example, when La or K is doped to Sr_2FeMoO_6 or Ba_2FeMoO_6, both of which are colossal magnetoresistance materials with high T_C, the composition of Fe valence states, Fe^{3+} and Fe^{2+}, is changed and T_C increases for La doping but decreases for K doping.[32–35] It will be thus interesting to explore the effects of *A*-site doping in a FM insulator La_2MnNiO_6 having the highest T_C. In fact, there was a report on *A*-site doping to this system,[36] in which a polar behavior in Lu-doped La_2MnNiO_6 has been examined. In this case, Lu doping gives *A*-site size disorder keeping the oxidation states fixed.

Recently, there was a report on Sr-doped $La_{2-x}Sr_xMnNiO_6$,[21] which corresponds to the effective hole-carrier doping to La_2MnNiO_6. When La^{3+} ions are switched by the Sr^{2+} ions, the valence states of Mn and Ni will be changed to keep the charge neutrality, which is distinct from the case of Lu doping. According to x-ray absorption spectroscopy (XAS) and x-ray magnetic circular dichroism (XMCD) experiment on Sr-doped $La_{2-x}Sr_xMnNiO_6$,[21] the measured Mn 2*p* XAS spectra for $x=0$ and $x=0.2$ are close to each other, but the XMCD signal for $x=0.2$ is substantially lower than for $x=0$. Possible antisite disorder of Mn/Ni ions at *B* sites was invoked as a main cause of such low XMCD signal for $x=0.2$. This speculation, however, remains to be verified.

In this paper, to explore the effects of *A*-site Sr doping and *B*-site antisite disorder in Sr-doped La_2MnNiO_6, we have studied electronic and magnetic properties of $La_{2-x}Sr_xMnNiO_6$, employing the *ab initio* band-structure method. We have investigated effects on the superexchange interaction between TM elements[5,23,30] and on the crystal structure. Interestingly, we have found that Sr doping induces the half-metallic feature in $La_{2-x}Sr_xMnNiO_6$, which is robust with respect to the antisite disorder at *B* sites.

II. METHODOLOGY

We have employed the full-potential linearized augmented plane-wave band method[37] implemented in WIEN2K package.[38] For the exchange-correlation energy functional, we used the generalized gradient approximation (GGA).[39] We have also investigated the effects of on-site Coulomb correlation *U* between TM 3*d* electrons in the GGA+*U* scheme.[40,41]

Monoclinic $P2_1/n$ structure of La_2MnNiO_6 is employed for the band-structure calculation.[6] Some of La ions in a supercell are replaced with Sr ions to describe the Sr doping. For $La_{2-x}Sr_xMnNiO_6$, we have considered a 40-atom supercell for $x=0.25$ and 20-atom supercells for $x=0.5$, 1.0, 1.5. For each doped system, the valence wave functions inside the muffin-tin spheres are expanded with spherical harmonics up to $l_{max}=10$. The wave function in the interstitial region is expanded with plane waves up to $K_{max}=7.0/R_{MT}$, where R_{MT} is the smallest muffin-tin sphere radius. R_{MT} were set as 2.5 a.u., 2.5 a.u., 1.6 a.u., 1.9 a.u., and 2.0 a.u. for La, Sr, O, Mn, and Ni, respectively. The charge density was expanded with plane waves up to $G_{max}=12$ $(a.u.)^{-1}$. We have used 1000 *k* points inside the first Brillouin zone. Especially for $La_{1.75}Sr_{0.25}MnNiO_6$, the atomic relaxation has been performed based on the experimental structure of undoped system with the restriction of Hellman-Feynman force of each atom is of order 1 mRy/a.u. Hence the smaller $R_{MT}=1.9$ a.u. is used for Ni of $La_{1.75}Sr_{0.25}MnNiO_6$ not to have overlapping spheres on the course of the relaxation. When exploring the effects of antisite disorder at *B* sites in $La_{2-x}Sr_xMnNiO_6$, we have adopted

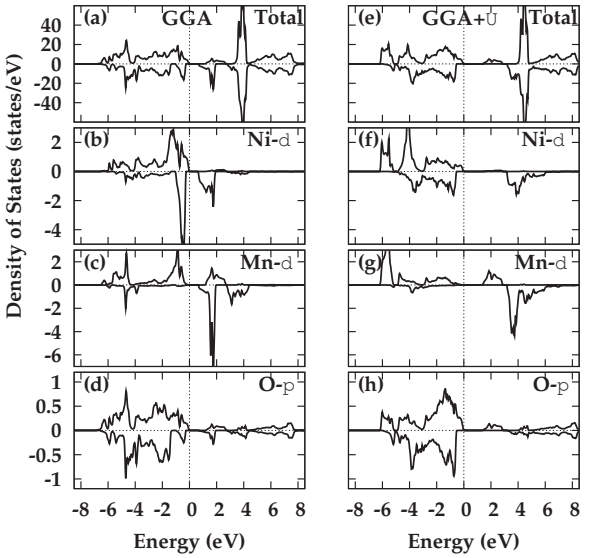

FIG. 1. Total and site-projected partial DOSs for La_2MnNiO_6. (a)–(d): DOS in the GGA and (e)–(h): DOS in the GGA+U with U=0.40 Ry (5.4 eV) for both Mn and Ni.

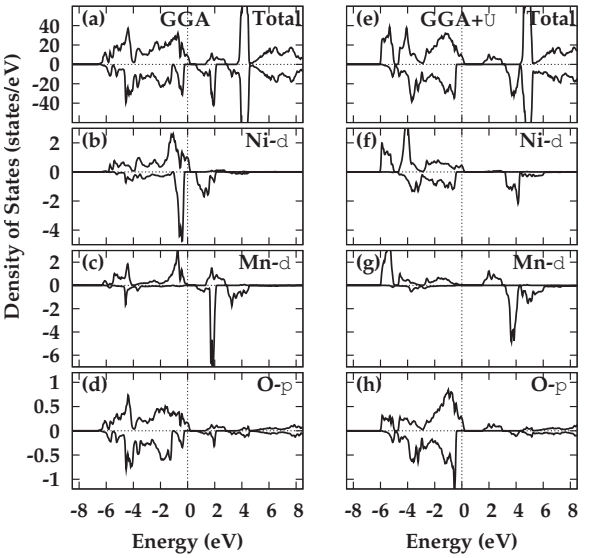

FIG. 2. Total and site-projected partial DOSs for $La_{1.75}Sr_{0.25}MnNiO_6$ (x=0.25). (a)–(d): DOS in the GGA and (e)–(f): DOS in the GGA+U with U=0.40 Ry (5.4 eV) for both Mn and Ni.

the virtual atom method in describing the A sites to save the computational time.

III. RESULTS AND DISCUSSIONS

A. Half-metallic electronic structure

Let us first discuss the electronic structure of undoped La_2MnNiO_6. Figure 1 provides the density of states (DOS) of La_2MnNiO_6 both in the GGA and the GGA+U band calculations. The GGA results were taken from our previous paper.[16] The electronic structures in the GGA are consistent with those in literature.[7,14] XAS study[21] indicated that the Coulomb correlation interactions of Mn 3d and Ni 3d electrons in La_2MnNiO_6 are very large. So we have also investigated electronic structures of La_2MnNiO_6 in the GGA+U scheme. In the GGA+U, U value of 0.40 Ry (5.4 eV) is selected. It is evident that the U effect strengthens the insulating nature of La_2MnNiO_6. Site-projected partial DOSs both in the GGA and the GGA+U suggest that the valence states of Ni and Mn are divalent (Ni^{2+}:d^8) and tetravalent (Mn^{2+}:d^3), respectively. Namely, the occupied electronic configurations for Ni and Mn are $(t_{2g\uparrow}^3 t_{2g\downarrow}^3 e_{g\uparrow}^2)$ and $(t_{2g\uparrow}^3)$, respectively, where $\uparrow$ and $\downarrow$ stand for the majority and minority spin states. The magnetic moments of Ni^{2+} and Mn^{4+} are, respectively, 1.47μ_B and 2.80μ_B in the GGA scheme whereas 1.67μ_B and 3.18μ_B in the GGA+U scheme. The increase in the magnetic moment of each TM ion is expected in the GGA+U, since the electrons become more localized.

When Sr is doped at A site, it is worthwhile to check how the doping affects the crystal structure. Note that undoped La_2MnNiO_6 has highly distorted monoclinic structure. For this purpose, we have performed the atomic-relaxation calculation for a supercell of $La_{1.75}Sr_{0.25}MnNiO_6$ (x=0.25) having the same monoclinic structure as La_2MnNiO_6. We have found that highly distorted nature of the mother material does not change much on doping. At around the Sr sites, the Mn-O-Ni angle increases from 158.6° to 159.1°, whereas, at around the La sites, the angle decreases to 158.2°. The average distances of Sr-O and La-O in doped system are about 2% larger and −0.6% smaller than that of La-O in the undoped system, respectively. All these atomic displacements suggest that the Sr doping does not induce the significant change in the crystal structure so that the distorted nature is retained for $La_{1.75}Sr_{0.25}MnNiO_6$.

Figure 2 shows the DOSs of $La_{1.75}Sr_{0.25}MnNiO_6$ (x=0.25) both in the GGA and the GGA+U. Note that Sr doping corresponds to the effective hole doping, and so, on Sr doping, the Fermi level E_F is expected to shift down in energy to make the system metallic. Indeed Fig. 2 manifests that $La_{1.75}Sr_{0.25}MnNiO_6$ becomes metallic with the finite DOS at E_F. Worth noting is that E_F crosses only the Ni DOS but not the Mn DOS, implying that hole carriers are produced only at Ni sites. Furthermore, E_F crosses only the majority spin states of Ni but not the minority spin states. That is, on Sr doping, electrons come out of the Ni^{2+} majority spin state which has originally $(t_{2g\uparrow}^3 t_{2g\downarrow}^3 e_{g\uparrow}^2)$ configuration. Hence in $La_{1.75}Sr_{0.25}MnNiO_6$, E_F crosses only the highest e_g majority spin states of Ni so as to exhibit half-metallic feature.

Note that there are several double perovskites exhibiting half-metallic feature. But those are mostly ferrimagnetic materials.[42–46] In this aspect, half-metallic $La_{2-x}Sr_xMnNiO_6$ with FM ordering of Mn and Ni magnetic moments is rather exceptional. The half-metallic feature is preserved both in the GGA and the GGA+U schemes. Due to large hybridization between oxygen p and TM d states, E_F also crosses the mixed O p states. Then the electron can hop from one Ni to the neighboring Ni through oxygen, all of which are in FM alignment. This situation is reminiscent of the double-exchange mechanism, in which only the majority-spin electron shows metallic behavior. Therefore, it is expected that the FM double-exchange interaction in the hole-doped sys-

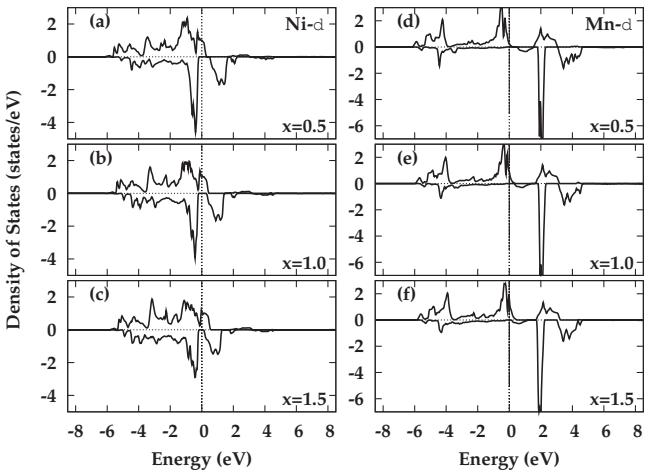

FIG. 3. Partial DOSs of Ni d and Mn d for $La_{2-x}Sr_xMnNiO_6$ with varying x in the GGA.

tem reinforces the FM ordering of TM elements, which is produced inherently by the FM superexchange interaction.

The magnetic moments of Ni and Mn ions are, respectively, $1.29\mu_B$ and $2.77\mu_B$ in the GGA scheme while $1.60\mu_B$ and $3.13\mu_B$ in the GGA+U scheme. The hole doping reduces the magnetic moments with respect to those for undoped La_2MnNiO_6, and the reduction in magnetic moment is stronger for Ni. The total magnetic moment per formula unit of $La_{1.75}Sr_{0.25}MnNiO_6$ is $9.500\mu_B$ both in the GGA and the GGA+U schemes, which is consistent with the configuration that Sr^{2+} ion has replaced one of the eight La^{3+} ions in the supercell of 40 atoms.

In Fig. 3 are shown the partial DOSs of Ni and Mn for $La_{2-x}Sr_xMnNiO_6$ with varying x. We have seen in Figs. 1 and 2 that the results in the GGA are physically the same as those in the GGA+U, and so we have employed the GGA band calculation in Fig. 3 to examine the effects of higher Sr doping. Even at the high substitution rate, the FM interaction between Mn and Ni ions is favored over the antiferromagnetic (AF) interaction. For example, the energy difference between AF and FM phases of $LaSrMnNiO_6$ ($x=1.0$) is obtained to be about 100 meV/f.u. Furthermore, as Sr-doping ratio increases, the half-metallic nature is strengthened, which results from the occupancy change in Ni $e_{g\uparrow}$ states. For $LaSrMnNiO_6$ ($x=1.0$), about half of the Ni e_g states become occupied so as to have the valence state of Ni^{3+} ($t_{2g}^6 e_g^1$). Then the anticipated magnetic moment would be $1\mu_B$, which is close to the calculated magnetic moment of $0.9\mu_B$. With increasing Sr doping, there appear finite Mn d majority spin states at E_F, but the amount of Mn d DOS crossing E_F is far less than that of Ni d DOS for $x \leq 0.5$. Still the half-metallic nature remains intact for whole doping range.

The variation in the magnetic moment of each TM ion on Sr doping is shown in Fig. 4. The magnetic moment of Ni changes significantly on Sr doping, but that of Mn does not change much. In the case of $LaSrMnNiO_6$ ($x=1.0$), the magnetic moment of Mn ion is $2.7\mu_B$, which does not change much from $2.8\mu_B$ of undoped La_2MnNiO_6, whereas the magnetic moment of Ni is changed a lot from $1.5\mu_B$ to $0.9\mu_B$. This feature is consistent with the variation in the partial DOSs in Fig. 3.

Figure 5 shows the charge-density difference (CDD) plot which corresponds to valence-charge density of the crystalline solid after subtraction of the superposed atomic charge density of the valence electrons. Figure 5(a) is the CDD around Ni site of the undoped La_2MnNiO_6 and Fig. 5(b) is that of $LaSrMnNiO_6$ ($x=1.0$). Likewise, Figs. 5(c) and 5(d) are the CDD plots around Mn site of La_2MnNiO_6 and $LaSrMnNiO_6$, respectively. The blue (dark) and the red (light) color refer to the minus (depleted) and the plus (accumulated) charge density in the solid with respect to the atomic charge density. The CDDs around TM ions show clearly the symmetrized orbital shapes that arise from the octahedral crystal field. For both Ni and Mn in La_2MnNiO_6, accumulated t_{2g} states in red and depleted e_g states in blue are apparent in Figs. 5(a) and 5(c). The Sr-doping effect is prominent when comparing Figs. 5(a) and 5(b), which shows that, on Sr doping, the electrons are coming out of the hybridized Ni e_g and O p states. On the contrary, there is almost no distinction between Figs. 5(c) and 5(d), reflecting that the electronic structure of Mn is hardly changed on Sr doping. The marked change in CDD only at Ni sites is again consistent with the DOS data given in Figs. 1–3.

B. Effects of antisite disorder at B sites

As mentioned in the introduction, the XMCD signal for $La_{2-x}Sr_xMnNiO_6$ ($x=0.2$) is substantially lower than for $x=0$, even though the line shape is very similar to each other.

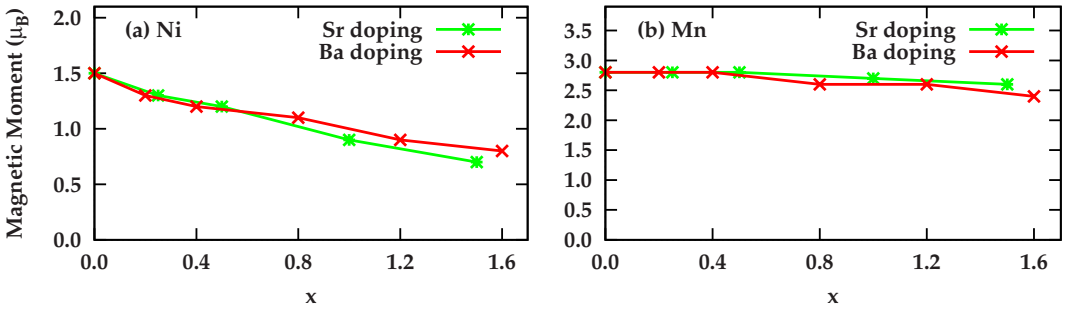

FIG. 4. (Color online) Ni and Mn magnetic moments as a function of doping of Sr or Ba to La_2MnNiO_6. Sr doping is considered in the supercell calculation, while Ba doping is treated in the virtual atom method. We have assumed a virtual atom $\widetilde{Lb}$ in $\widetilde{Lb}_2MnNiO_6$ with effective atomic number $Z_x=57(2-x)+56x$. Both calculation is in the GGA scheme.

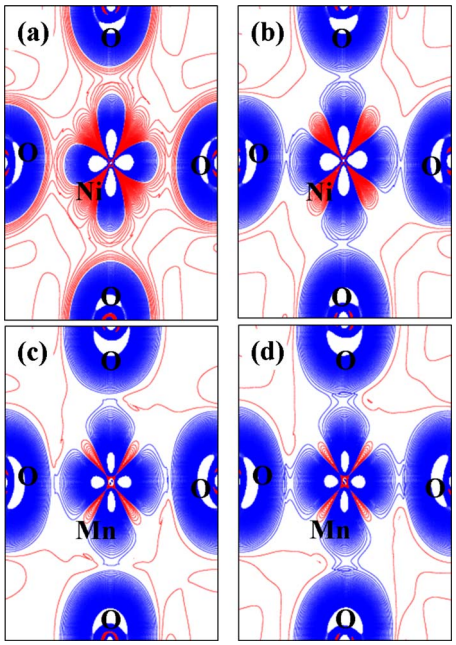

FIG. 5. (Color online) Top: CDD plot around Ni site. (a) La_2MnNiO_6 and (b) $LaSrMnNiO_6$. Bottom: CDD plot around Mn site. (c) La_2MnNiO_6 and (d) $LaSrMnNiO_6$. Both doped and undoped cases are performed using GGA functional.

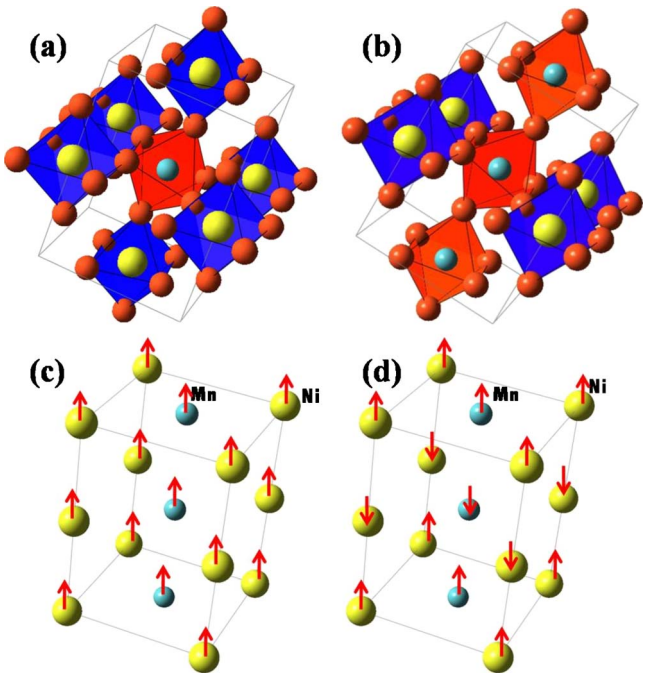

FIG. 6. (Color online) (a) $\widetilde{Lb}_2MnNiO_6$ with ordered Mn/Ni. (b) $\widetilde{Lb}_2MnNiO_6$ with Mn/Ni antisite disorder. (c) Assumed FM spin configuration for the disordered system (b). (d) Assumed AF spin configuration for the disordered system (b).

The weak XMCD signal for $x=0.2$ with respect to that for $x=0$ was attributed to the antisite disorder of Mn/Ni ions at B sites. According to recent experimental reports on La_2MnNiO_6 thin film,[23–25] the antisite disorder exists at B sites even for undoped system, which affects structural and magnetic properties of the film system.

We have thus examined the effect of the antisite disorder on electronic and magnetic properties of $La_{2-x}Sr_xMnNiO_6$, by performing the band-structure calculations for a system with incomplete ordering of Ni and Mn ions at B sites. To simulate Sr doping at A sites for these band calculations, we employed the virtual atom method, instead of the supercell calculation. In the virtual atom method, Ba doping to La_2MnNiO_6 is considered instead of Sr, assuming that Ba doping would produce essentially the same hole-doping effects as Sr doping. Then, for $La_{2-x}Ba_xMnNiO_6$, the virtual atom $\widetilde{Lb}$ in $\widetilde{Lb}_2MnNiO_6$ is assumed to have the effective atomic number $Z_x=57(2-x)+56x$. By using the virtual atom method, the computational time is saved a lot for a present system having disorder both at A and B sites.

We have checked first whether the results of the virtual atom method applied to A-site-doped systems are really consistent with those of the supercell calculation. In this case, we consider the systems with perfect ordering of Ni/Mn ions at B sites. In fact, the overall electronic structures obtained from the virtual atom method are very similar to those of the supercell calculation, and the doping-induced transition from a FM insulating phase to a half-metallic phase is also well reproduced by the virtual atom method. Furthermore, as shown in Fig. 4, calculated magnetic moments of Ni and Mn in the virtual atom method for $\widetilde{Lb}_2MnNiO_6$ are obtained to be quite close to those in the supercell calculation for $La_{2-x}Sr_xMnNiO_6$. These results demonstrate that the virtual atom method yields good approximate results that are consistent with those of the supercell calculation.

The structural stability with introducing A-site doping is also checked within the virtual atomic scheme. We consider an idealized structure of $\widetilde{Lb}_2MnNiO_6$ in which each oxygen atom is located at the midposition between two TM atoms, while $\widetilde{Lb}$ atoms are located at the midposition between neighboring oxygen atoms. Then TM-O-TM angle for an idealized structure is 180°, which is far different from 158.6° of the original distorted structure of La_2MnNiO_6. Total-energy calculation provides that the real distorted structure is more stable than the ideal one by more than 300 meV/f.u. for whole doping range, which indicates that the original distorted structure will be retained on doping.

Now let us consider the electronic structures of virtual system $\widetilde{Lb}_2MnNiO_6$ with Mn/Ni antisite disorder at B sites. In the ordered system, each Mn (Ni) ion has six neighboring Ni (Mn) ions [see Fig. 6(a)]. For an antisite disordered system, we considered a specific configuration of $\widetilde{Lb}_2MnNiO_6$ with $Z_{x=0.2}$, in which each Mn (Ni) ion has four neighboring Ni (Mn) and two neighboring Mn (Ni) ions, as shown in Fig. 6(b). The mother material La_2MnNiO_6 is a FM insulator, in which the FM superexchange interaction is favored between neighboring Mn and Ni sites.[16] When the perfect order of Mn and Ni is somehow changed, as in Fig. 6(b), the interaction between neighboring Mn-Mn and Ni-Ni sites will also become important. According to the GKA rules,[3,4] the superexchange interaction between filled orbitals favors the AF order. So the exchange interaction between Mn^{4+} and Mn^{4+} with filled t_{2g}^3 will be AF. Likewise, the interaction between

TABLE I. Total energy for $\widetilde{Lb}_2MnNiO_6$ with a virtual atom $\widetilde{Lb}$ with $Z_{x=0.2}$. Total energies are calculated in the GGA scheme for Mn/Ni ordered (O) and disordered (D) $\widetilde{Lb}_2MnNiO_6$ systems. Total energy of DFM $\widetilde{Lb}_2MnNiO_6$ is set to be zero.

	Ordered FM (OFM)	Disordered FM (DFM)	Disordered AF (DAF)
Energy (meV)	−110	0	4.6

Ni^{2+} and Ni^{2+} with filled e_g^2 will also be AF. As a consequence, the situation for a system with *B*-site disorder becomes complicated due to the presence of both the FM interaction between different TM ions and the AF interaction between the same TM ions.

Keeping the FM ordering between Mn and Ni sites, we have compared energetics for two cases of FM and AF orderings between the same TM ions, as shown in Figs. 6(c) and 6(d). The result is summarized in Table I. The FM phase of $\widetilde{Lb}_2MnNiO_6$ with perfect Mn/Ni order (OFM) has the lowest total energy. However, when there exists Mn/Ni antisite disorder, the energy difference between two spin configurations of disordered FM (DFM) and disordered AF (DAF) states becomes very small (4.6 meV/f.u.), even though the DFM state is still more stable. Antisite disorder is supposed to be generated during the sample-making process.[21] The XMCD experiment for $La_{1.8}Sr_{0.2}MnNiO_6$ was performed at around 80 K, which corresponds to thermal energy of 6.9 meV. This experimental temperature energy scale is of the same order as the energy difference between two spin configurations (DFM and DAF) of the antisite disordered system. Then both the FM and the AF spin orderings would coexist between the same TM ions, and so the XMCD signal will be much suppressed.

On the other hand, despite the different atomic orderings and spin configurations in Fig. 6, the overall DOSs for three cases, OFM, DFM, and DAF, are similar to one another, as presented in Fig. 7. This implies that the small antisite disorder at *B* sites does not modify the electronic properties of the system much, even though the small portion of the magnetic exchange interaction between TM elements is changed. This finding explains why the observed XAS for $x=0$ and $x=0.2$ is close to each other while the XMCD signal for $x=0.2$ is substantially lower than for $x=0$. One more thing to note in Fig. 7 is that the half metallicity is seen to be slightly broken for the DAF case. However, considering that the DFM phase is more stable than the DAF phase, one can safely say that the half-metallic nature of $La_{2-x}Sr_xMnNiO_6$ system is robust against the antisite disorder at *B* sites.

In the above calculations for $La_{2-x}Sr_xMnNiO_6$ with antisite disorder at *B* sites, we have assumed the original distorted monoclinic structure of La_2MnNiO_6. But it needs to be examined whether the antisite disorder releases the distorted

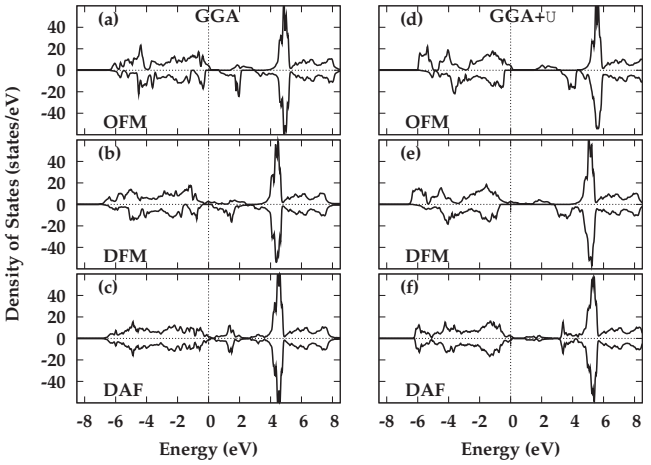

FIG. 7. Total DOSs for $\widetilde{Lb}_2MnNiO_6$ with $Z_{x=0.2}$ with antisite disorder at *B* sites in the virtual atom method. (Left) DOSs in the GGA and (right) DOSs in the GGA+*U* scheme.

structural nature of La_2MnNiO_6 or not. Hence the same calculation has been performed for an idealized structure, in which oxygen atoms are located at the midposition between TM atoms. Both DFM and DAF phases with idealized structure are found to have much higher energies than those with distorted structure by more than 300 meV/f.u., indicating that the antisite disorder at *B* sites would not change the distorted structural nature significantly. Further, we have obtained that, for the above assumed antisite disorder, the energy difference between DFM and DAF phases with idealized structure (~ 2 meV) is less than half of that with the distorted structure (4.6 meV). This reflects that the distortion acts to favor the FM interaction over the AF interaction in the presence of antisite disorder.

IV. CONCLUSION

We have investigated electronic structures and magnetic properties of hole-carrier-doped $La_{2-x}Sr_xMnNiO_6$ by performing the *ab initio* band-structure calculation. On Sr doping, the material shows robust half-metallic behavior. The metallic behavior comes mostly from the hole carriers which are created in the e_g majority-spin states of Ni.

We have also checked that both the *A*-site Sr doping and the antisite disorder at *B* sites do not change the distorted structural nature and the FM exchange interaction between Mn and Ni in $La_{2-x}Sr_xMnNiO_6$. We have verified that the possible antisite disorder at *B* sites in a Sr-doped system can be a reason of the substantially weak XMCD signal, as compared to the undoped system.

ACKNOWLEDGMENTS

This work was supported by the NRF (Grant No. 2009-0079947) and by the POSTECH BK21 Physics Division.

[1] G. Blasse, J. Phys. Chem. Solids **26**, 1969 (1965).
[2] K. Asai, H. Sekizawa, and S. Iida, J. Phys. Soc. Jpn. **47**, 1054 (1979).
[3] J. B. Goodenough, *Magnetism and the Chemical Bond* (Wiley, New York, 1963).
[4] D. Khomskii, *Spin Electronics*, Springer Lecture Notes in Physics Vol. 569, edited by M. Ziese and M. J. Thornton (Springer, New York, 2001), Chap. 5.
[5] R. I. Dass, J.-Q. Yan, and J. B. Goodenough, Phys. Rev. B **68**, 064415 (2003).
[6] N. S. Rogado, J. Li, A. W. Sleight, and M. A. Subramanian, Adv. Mater. **17**, 2225 (2005).
[7] S. F. Matar, M. A. Subramanian, A. Villesuzanne, V. Eyert, and M.-H. Whangbo, J. Magn. Magn. Mater. **308**, 116 (2007).
[8] H. Guo, J. Burgess, S. Street, A. Gupta, T. G. Calvarese, and M. A. Subramanian, Appl. Phys. Lett. **89**, 022509 (2006).
[9] M. Hashisaka, D. Kan, A. Masuno, M. Takano, Y. Shimakawa, T. Terashima, and K. Mibu, Appl. Phys. Lett. **89**, 032504 (2006).
[10] M. P. Singh, C. Grygiel, W. C. Sheets, Ph. Boullay, M. Hervieu, W. Prellier, B. Mercey, Ch. Simon, and B. Raveau, Appl. Phys. Lett. **91**, 012503 (2007).
[11] S. Zhou, L. Shi, H. Yang, and J. Zhao, Appl. Phys. Lett. **91**, 172505 (2007).
[12] M. N. Iliev, H. Guo, and A. Gupta, Appl. Phys. Lett. **90**, 151914 (2007).
[13] H. Z. Guo, J. Burgess, E. Ada, S. Street, A. Gupta, M. N. Iliev, A. J. Kellock, C. Magen, M. Varela, and S. J. Pennycook, Phys. Rev. B **77**, 174423 (2008).
[14] H. Das, U. V. Waghmare, T. Saha-Dasgupta, and D. D. Sarma, Phys. Rev. Lett. **100**, 186402 (2008).
[15] P. Padhan, H. Z. Guo, P. LeClair, and A. Gupta, Appl. Phys. Lett. **92**, 022909 (2008).
[16] B. Kim, J. Lee, B. H. Kim, H. C. Choi, K. Kim, J.-S. Kang, and B. I. Min, J. Appl. Phys. **105**, 07E515 (2009).
[17] J.-S. Kang, G. Kim, H. J. Lee, S. Kolesnik, B. Dabrowski, H. Lee, J.-Y. Kim, J. Lee, B. Kim, and B. I. Min, J. Appl. Phys. **105**, 07D721 (2009).
[18] H. Das, U. V. Waghmare, T. Saha-Dasgupta, and D. D. Sarma, Phys. Rev. B **79**, 144403 (2009).
[19] M. Kitamura, I. Ohkubo, M. Kubota, Y. Matsumoto, H. Koinuma, and M. Oshima, Appl. Phys. Lett. **94**, 132506 (2009).
[20] M. N. Iliev, M. M. Gospodinov, M. P. Singh, J. Meen, K. D. Truong, P. Fournier, and S. Jandl, J. Appl. Phys. **106**, 023515 (2009).
[21] J.-S. Kang, H. J. Lee, D. H. Kim, S. Kolesnik, B. Dabrowski, K. Swierczek, J. Lee, B. Kim, and B. I. Min, Phys. Rev. B **80**, 045115 (2009).
[22] M. Kitamura, I. Ohkubo, M. Matsunami, K. Horiba, H. Kumigashira, Y. Matsumoto, H. Koinuma, and M. Oshima, Appl. Phys. Lett. **94**, 262503 (2009).
[23] M. P. Singh, K. D. Truong, S. Jandl, and P. Fournier, Phys. Rev. B **79**, 224421 (2009).
[24] H. Guo, A. Gupta, M. Varela, S. Pennycook, and J. Zhang, Phys. Rev. B **79**, 172402 (2009).
[25] K. D. Truong, M. P. Singh, S. Jandl, and P. Fournier, Phys. Rev. B **80**, 134424 (2009).
[26] J. B. Goodenough, A. Wold, R. J. Arnott, and N. Menyuk, Phys. Rev. **124**, 373 (1961).
[27] M. Sonobe and K. Asai, J. Phys. Soc. Jpn. **61**, 4193 (1992).
[28] M. C. Sánchez, J. García, J. Blasco, G. Subias, and J. Perez-Cacho, Phys. Rev. B **65**, 144409 (2002).
[29] J. Blasco, M. C. Sánchez, J. Perez-Cacho, J. Garcia, G. Subias, and J. Campo, J. Phys. Chem. Solids **63**, 781 (2002).
[30] V. L. Joseph Joly, P. A. Joy, S. K. Date, and C. S. Gopinath, Phys. Rev. B **65**, 184416 (2002).
[31] C. L. Bull, D. Gleeson, and K. S. Knight, J. Phys.: Condens. Matter **15**, 4927 (2003).
[32] G. Kim, S. S. Lee, S. C. Wi, J.-S. Kang, S. W. Han, J. Y. Kim, B. W. Lee, J. Y. Kim, H. J. Shin, B. G. Park, J.-H. Park, and B. I. Min, J. Appl. Phys. **99**, 08Q309 (2006).
[33] J. Navarro, C. Frontera, Ll. Balcells, B. Martinez, and J. Fontcuberta, Phys. Rev. B **64**, 092411 (2001).
[34] H. M. Yang, W. Y. Lee, H. Han, B. W. Lee, and C. S. Kim, J. Appl. Phys. **93**, 6987 (2003).
[35] J. Kim, J. G. Sung, H. M. Yang, and B. W. Lee, J. Magn. Magn. Mater. **290–291**, 1009 (2005).
[36] D. J. Singh and C. H. Park, Phys. Rev. Lett. **100**, 087601 (2008).
[37] M. Weinert, E. Wimmer, and A. J. Freeman, Phys. Rev. B **26**, 4571 (1982); H. J. F. Jansen and A. J. Freeman, *ibid.* **30**, 561 (1984).
[38] P. Blaha, K. Schwarz, G. K. H. Madsen, D. Kvasnicka, and J. Luitz, WIEN2k (Technische Universität Wien, Austria, 2001).
[39] J. P. Perdew, K. Burke, and M. Ernzerhof, Phys. Rev. Lett. **77**, 3865 (1996).
[40] V. I. Anisimov, I. V. Solovyev, M. A. Korotin, M. T. Czyzyk, and G. A. Sawatzky, Phys. Rev. B **48**, 16929 (1993).
[41] A. I. Liechtenstein, V. I. Anisimov, and J. Zaanen, Phys. Rev. B **52**, R5467 (1995).
[42] K.-I. Kobayashi, T. Kimura, H. Sawada, K. Terakura, and Y. Tokura, Nature (London) **395**, 677 (1998).
[43] W. E. Pickett, Phys. Rev. B **57**, 10613 (1998).
[44] J. H. Park, S. K. Kwon, and B. I. Min, Phys. Rev. B **65**, 174401 (2002).
[45] Y. K. Wang and G. Y. Guo, Phys. Rev. B **73**, 064424 (2006).
[46] J. H. Park, S. K. Kwon, and B. I. Min, J. Magn. **12**, 64 (2007).